The Journal of Chemical Physics

RESEARCH ARTICLE | SEPTEMBER 11 2023

Polyzwitterion fast and slow mode behavior are coupled to phase separation as observed by dynamic laser light scattering

Phillip D. Pickett ; Yuanchi Ma ; Vivek M. Prabhu

J. Chem. Phys. 159, 104902 (2023)
https://doi.org/10.1063/5.0162376

AIP Publishing

The Journal of Chemical Physics ARTICLE pubs.aip.org/aip/jcp

Polyzwitterion fast and slow mode behavior are coupled to phase separation as observed by dynamic laser light scattering

Cite as: J. Chem. Phys. 159, 104902 (2023); doi: 10.1063/5.0162376
Submitted: 14 June 2023 • Accepted: 18 August 2023 •
Published Online: 11 September 2023

Phillip D. Pickett, Yuanchi Ma,[a] and Vivek M. Prabhu[b]

AFFILIATIONS

Materials Science and Engineering Division, Material Measurement Laboratory, National Institute of Standards and Technology, Gaithersburg, Maryland 20899, USA

[a]**Present address:** Department of Polymer Science and Engineering, Qingdao University of Science and Technology, Qingdao, Shandong, China.
[b]**Author to whom correspondence should be addressed:** vprabhu@nist.gov

ABSTRACT

A model zwitterionic polysulfobetaine, poly(3-(acrylamidopropyl-dimethyl-ammonium) propyl-1-sulfonate) (pAPAPS), phase separates upon cooling and exhibits an upper critical solution temperature (UCST) behavior with no added salt in deuterium oxide solutions. Dynamic light scattering measurements indicate the presence of distinct fast and slow diffusive modes, where the fast mode is interpreted as a collective diffusion coefficient and the slow mode is attributed to the diffusion of multi-chain dynamic clusters. The relative population of fast and slow modes varies systematically with temperature and concentration. A clustering temperature (T^*) was assigned when the slow mode first appeared upon cooling. The slow mode then increases in relative scattering amplitude as the phase boundary is approached. The fast mode exhibits a concentration dependence above T^* consistent with the virial expansion in the collective diffusion. The sign of the virial coefficient (k_d) is negative, even in the good solvent region above the expected Flory temperature ($\Theta \approx 39\ ^\circ$C), a behavior distinct from synthetic neutral polymers in organic solvents. The onset of multi-chain clustering at $T < T^*$ coincides with the poor solvent regime ($T < \Theta$). Attractive dipolar interactions due to the zwitterionic sulfobetaine groups in pAPAPS are suggested as the origin of the multi-chain clusters with no salt. Upon the addition of 100 mM NaCl, the slow mode is suppressed, and the hydrodynamic radius is consistent with polyzwitterion chain dimensions in a dilute solution. We find that concentration dependent diffusion is highly linked to the theta temperature and the emergence of dynamic clusters as the polymer goes from good to poor solvent on approach to the UCST. The slow mode in the semidilute regime is reported along with preliminary small-angle neutron scattering data that show salt reduces clustering and leads to predominantly chain scattering.

Published by AIP Publishing. https://doi.org/10.1063/5.0162376

I. INTRODUCTION

The solution properties of polyzwitterions make them important for biomedical, environmental, cosmetic, coating, and thin-film applications.[1–5] In particular, polyzwitterions exhibit ionic strength and temperature responsive phase behavior in water.[5–13] In the absence of salt, the zwitterionic functional groups lead to a collapsed state of the polymer chains due to strong dipolar attractions.[14,15] Upon addition of salt, chain dimensions increase, known as the anti-polyelectrolyte effect,[13,15–17] with origins due to a weakening of the dipolar attraction and selective adsorption of salt ions that increases the net charge and induces repulsive intra-chain electrostatic interactions.[18] Further addition of salt leads to reduced chain dimensions due to screening of repulsive interactions and good solvent behavior. This behavior contrasts highly charged, intrinsically-flexible polyelectrolytes, such as sodium poly(styrene sulfonate), that show expanded dimensions at very low ionic strength, and the addition of salt leads to chain contraction due to screening of the repulsive electrostatic interactions.[19,20] It should be clarified that the state of net charge depends upon the isoelectric point of the zwitterionic group and, therefore, may be highly pH dependent.[7,14] The strength of the dipolar interactions of polyzwitterions may also be reduced by increasing temperature since many polyzwitterions exhibit phase separation upon cooling, or upper critical solution temperature (UCST) behavior.[6,8,10,16]

Phase diagrams of polyzwitterions are of interest since they summarize the temperature, salt, or polymer concentration dependent boundaries between one and two phases in solution. Hildebrand and co-workers[8,21,22] studied the phase diagrams of a variety of polyzwitterions and reported a plateau in cloud point temperature up to a polymer concentration of 50 mg/ml. The cloud point decreases with increasing NaCl or NaBr salt concentration, consistent with a general increase in solvent quality. Huglin and Radwan have reported phase diagrams of polyzwitterions with a fixed concentration of NaCl for a variety of molar masses of methacrylate-based polysulfobetaines and observed that the critical temperature increased with increasing molar mass in a manner predicted by the Flory Huggins theory.[23] Mary *et al.*[24] reported phase diagrams for similar molar masses of the same polysulfobetaine and were able to demonstrate the influence of salt on the critical temperature for differing molar masses, in which the critical temperature of a higher molar mass polyzwitterion can be shifted to match that of a lower molar mass via the addition of salt. These studies highlight that the phase behavior of polyzwitterions exhibits sensitive dependence on salt concentration and relies on several factors that may occur on smaller length scales prior to macrophase separation. Still, the mechanism of phase separation in polyzwitterions is poorly understood, but additional measurements from the dynamics provide insight into the interactions.

Niu *et al.* observed two distinct diffusive modes in a zwitterionic polycarboxybetaine by dynamic light scattering (DLS),[14] where the ionic state is sensitive to the solution pH, at extremely low concentrations. A low amplitude slow mode was assigned to interchain aggregation. Wang and co-workers studied the salt dependent self-diffusion at the single-chain level of a polysulfobetaine via fluorescence correlation spectroscopy (FCS).[15] They observed a slight change in the diffusion coefficient between 0.01 mM and 0.1M salt but a large decrease in the diffusion coefficient from 0.1 to 1M salt. This was attributed to the swelling of the polyzwitterion chain (anti-polyelectrolyte effect) as the intrachain dipolar attractions are reduced at higher salt concentrations. Delgado and Schlenoff studied a Hofmeister series of salts with DLS and also observed anti-polyelectrolyte behavior.[13] They estimated the temperature-dependent hydrodynamic radius (R_h) at a fixed polymer concentration and observed two modes with no added salt. The fast mode dimensions did not vary with temperature and was assigned as a soliton motion of neighboring zwitterionic side groups with dimensions of 6 nm, while the slow mode at high temperatures was assigned to single chains, which then increased in size at lower temperatures, attributed to associations. In the no added salt limit, the slow mode persisted at higher temperatures, but the relative scattering amplitudes of the fast vs slow modes were not discussed. To note, the number-average molar mass of the poly(3-[2-(acrylamido) ethyldimethylammonio] propanesulfonate), PAEDAPS, was 5.05×10^5 g/mol in this case. Cao and Zhang reported a fast and slow mode in the relaxation time distributions of diffusing vinylpyridinium-based polysulfobetaine chains via DLS, which measures the collective diffusion coefficient. They attributed the fast mode to single chains and the slow mode to dynamic inhomogeneity due to interchain electrostatic repulsions, as supported by sedimentation velocity measurements.[25] The addition of salt below 100 mM NaCl highlighted effective charging of the chains due to asymmetric adsorption of counterions, while salt concentrations above 100 mM NaCl resulted in effective screening of charges and a decrease in electrostatic repulsive interactions, leading to the expected anti-polyelectrolyte behavior. Between no salt and 100 mM salt, the diffusion coefficients of the slow and fast modes only slightly vary. These studies illustrate the mediating role salt has on dynamics. However, in all these examples, the polymer concentration was held constant, and the identity of the collective diffusive modes as measured by DLS varies by study.

The self-diffusion coefficient measured by Wang and co-workers[15] using FCS directly reflects the dye-labeled chain transport and was attributed to a weakening of the dipolar attractions with a higher salt concentration [smaller Debye screening length (κ^{-1})]. However, the effect of polymer concentration on the diffusion coefficient was not studied. Additionally, the reported R_h under extreme dilutions (1×10^{-8} mol/l) should provide single chain behavior. At a finite concentration, the diffusion coefficient is influenced by thermodynamic interactions and hydrodynamics (viscosity effects). This is a well-studied problem for neutral polymer chains in good solvents, led by refinements of polymer models.[26–29] However, in the case of ion-containing polymers, such as polyzwitterions, such a framework is complicated by electrostatic interactions that can lead to multiple diffusive modes, even in dilute solutions.[30–32]

The interrelationship between the two modes in polyzwitterions and the solvent quality (phase separation) is poorly understood. Therefore, this work focuses on determining when the dipolar attractive interactions couple to phase separation using a model polysulfobetaine, poly(3-(acrylamidopropyl-dimethyl-ammonium) propyl-1-sulfonate) (pAPAPS). This system was chosen because the state of zwitterionic charge is not pH dependent due to the strongly acidic nature of the sulfonate and the permanent charge of the quaternized ammonium. The acrylamide monomer was chosen due to its resistance to hydrolysis, as opposed to the acrylate or methacrylate-based monomer. DLS measures the collective diffusion coefficient as a function of temperature and concentration, which reveals sensitive shifts between chain transport and multi-chain dynamic cluster populations in the one phase region on approach to the phase boundary (cloud point). Below the overlap concentration, a virial expansion in the collective diffusion coefficient was applied for the fast mode. The sign of the dynamic virial coefficient (k_d) unexpectedly appears negative under both good and poor solvent conditions.[33] The DLS measurements in the poor solvent domain show strong deviations from the inverse temperature dependence of k_d. An alternate model is required that considers multi-chain clusters that enhance the attractions among chains, leading to a strongly negative k_d in the absence of salt.

II. EXPERIMENTAL

A. Materials

The synthesis of the zwitterionic monomer, 3-(acrylamidopropyl-dimethyl-ammonium) propyl-1-sulfonate (APAPS), and the homopolymer (pAPAPS) used the following reagents: 1,3-Propanesultone (TCI America, >99%), 2,2′-Azobis [2-(2-imidazolin-2-yl)propane]dihydrochloride (VA-044) (Wako, granule, stored at −10 °C), benzene sulfonic acid (Sigma-Aldrich, 98%), NaCl (Sigma-Aldrich, >99%), acetone (JT Baker), and methanol (Sigma-Aldrich, anhydrous, 99.8%) were all used as received. *N*-[3-(dimethylamino)propyl]acrylamide (DMAPA)

(>98%) was supplied from TCI America and distilled prior to use. 4-Cyano-4 (ethylsulfanylthiocarbonylsulfanyl)-pentanoic acid (CEP) was synthesized according to the literature procedures.[34] Detailed synthesis procedures for APAPS and CEP are in the supplementary material. Deuterium oxide (D_2O) (Cambridge Isotope Laboratories, 99.9% D atom) was used as received.

B. Characterization

The APAPS monomer was analyzed via proton and carbon nuclear magnetic resonance (NMR) spectroscopy (^{1}H-NMR and ^{13}C-NMR, respectively) for its structure and purity using a Bruker 600 UltraShield spectrometer operated by a combination of TopSpin 3.2 and IconNMR Automation software. The model polysulfobetaine homopolymer was synthesized by aqueous reversible addition-fragmentation chain transfer (RAFT) polymerization of APAPS (Scheme S3). The percent monomer conversion of the polymerization of APAPS was monitored by ^{1}H-NMR spectroscopy using a benchtop Spinsolve 80 carbon model spectrometer manufactured by Magritek and operated using Spinsolve Software version 1.15.1. The sample was run in D_2O containing a 0.05 volume fraction of tetramethylsilane (TMS) as an internal standard. The data were collected using 32 scans at a 90° pulse angle with a 6.4 s acquisition time and a 7 s repetition time. The homopolymer pAPAPS was characterized by aqueous size exclusion chromatography (SEC) using 0.2M LiBr/20% acetonitrile in water as the eluent at 30 °C and a flow rate of 0.3 ml/min. SEC was performed with a Waters 1515 Isocratic HPLC Pump equipped with a Waters 717 Autosampler, a Waters 2487 Dual λ Absorbance Detector (264 nm), and a Waters 2414 Refractive Index Detector (30 °C) in series with TOSOH Biosciences TSK-GEL columns (Super AW3000, Super AW4000, and Super AW-L). The SEC instrument was interfaced using the Waters Breeze v3.30 software. The pAPAPS had a number-average relative molar mass (M_n) of 19 700 Da and a polydispersity ($\tilde{D}$) of 1.16 relative to poly(styrene sulfonate) calibration standards (Scientific Polymer Products). The ^{1}H-NMR and narrow and unimodal SEC traces of the pure pAPAPS are shown in Fig. S5.

Temperature dependent dynamic light scattering measurements at a scattering angle (θ) of 90° were conducted with a solid-state laser with a wavelength (λ) of 532 nm operating at 100 mW, but the laser power on the sample was lower due to neutral density filters. The scattered light was collected by single-mode fiber optics, split into separate single photon counting modules, and cross correlated by a Brookhaven Instruments correlator (TurboCorr). Two sets of DLS data were collected: (1) a temperature dependent experiment in which 1 ml of a pAPAPS solution at various concentrations in D_2O was filtered via a 0.45 μm PVDF filter into a cuvette and equilibrated at an elevated temperature (56 °C for 4 mg/ml to 12 mg/ml and 68 °C for 20 mg/ml to 300 mg/ml) for 45 min. After data collection for 30 min, the temperature was ramped at 2 °C/min from high temperature to low temperature at 2 °C increments with a 5 min equilibration time and a total data collection time of 30 min at each temperature; and (2) a temperature cycle experiment in which 1 ml of an 8 mg/ml sample of pAPAPS in D_2O was filtered via a 0.45 μm PVDF filter into a cuvette and equilibrated at 50 °C for 2 h. The temperature was then lowered at a 5 °C/min ramp rate to subsequent temperatures at 1 °C increments down to 40 °C with a 5 min equilibration time and 15 min data collection time at each temperature. The temperature was then incrementally increased back to 50 °C while collecting data using the same steps. Samples were housed in a Quantum Northwest q-Pod unit with ±0.1 °C precision and a Quantum Northwest TC125 temperature controller. The chamber was continuously purged with dry nitrogen for measurements at temperatures approaching the dew point. Cloud point temperatures were determined separately with the same experimental setup by using the laser light transmission measured by a Thorlabs PM100D photodiode detector. The samples were cooled at a ramp rate of 0.2 °C/min, with data collected every 5 s. The inflection points determined by the differentiation of the transmission curves were assigned the cloud point temperature.

Angular-dependent DLS measurements used a modified Brookhaven Instruments BI-200SM goniometer with a 2 W coherent VERDI diode-pumped solid-state laser with λ = 532 nm operating at 100 mW. The solutions of pAPAPS at 8 mg/ml were measured in D_2O and 100 mM NaCl in D_2O at 10, 15, 20, 30, 40, and 50 °C. These measurements were collected at scattering angles of 60°, 75°, 90°, 105°, and 120°. The pinhole just before the detector was adjusted to 400 μm for 0M NaCl samples and 1 mm for 100 mM NaCl samples. The temperature was controlled using an external recirculating bath. Selected static light scattering measurements on pAPAPS at 8 mg/ml in D_2O were measured at 50 °C at scattering angles between 30° and 140° in 5° increments with a 1 mm pinhole. This data was scaled to the small-angle neutron scattering (SANS) data as shown in the supplementary material.

SANS measurements were performed on the NGB-30m SANS beam line at the National Institute of Standards and Technology Center for Neutron Research (NCNR). The wavelength of the neutron (λ) was 6.0 Å, with a wavelength spread (Δλ/λ) of 13.8%. The desired sample was transferred to a 1.5 ml microcentrifuge tube and allowed to centrifuge for 5 min at 13 000 rpm. This sample was then transferred to another 1.5 ml microcentrifuge tube prior to loading into clean cylindrical Hellma Analytics QS-type quartz cells and mounting in a thermoelectric temperature-controlled heating block at 50 °C. The scattered intensity, $I(q)$, was measured as a function of the scattering vector (q), where $q = (4\pi/\lambda)\sin(\theta/2)$ and θ is the scattering angle. The 2D scattering patterns were reduced and placed onto absolute intensity units as described elsewhere.[33,35]

III. RESULTS AND DISCUSSION

A. General phase behavior of salt-free pAPAPS solutions

The phase separation behavior of pAPAPS [Fig. 1(a)] was conducted in D_2O to allow comparisons with SANS measurements of the radius of gyration (R_g) and second virial coefficient (A_2) and avoid quantitative shifts in thermal transitions due to isotopic effects.[33] The cloud point temperature as a function of polymer concentration (c) was determined from the inflection point of the transmittance of laser light through pAPAPS in D_2O solutions as a function of cooling. Figure 1(b) shows examples of the laser transmittance curves used to determine the cloud points. Figure 1(c) summarizes the temperature-polymer concentration cloud point diagram and UCST behavior. Above the UCST, one phase (1-Φ) is observed, and below the cloud point temperature, pAPAPS enters

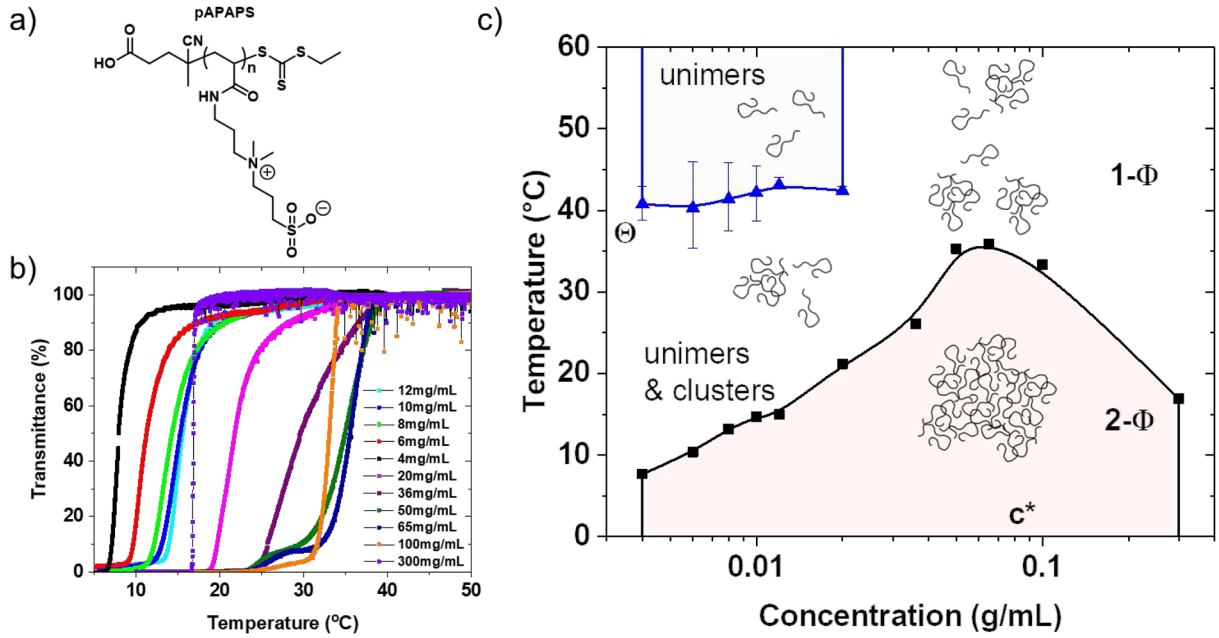

FIG. 1. (a) Chemical structure of pAPAPS; (b) Transmittance vs temperature curves for pAPAPS at various polymer concentrations; and (c) Upper critical solution temperature behavior of pAPAPS in D_2O defined by the cloud point temperatures (■) below, which is the two-phase region (2-Φ). The Flory theta temperature (Θ ≈ 39 °C) and chain overlap concentration (c^* = 82 mg/ml) are shown as references for the expected good to poor solvent quality and dilute to semi-dilute solution regimes, respectively. The cluster temperatures (blue triangle) were determined by the onset of the slow mode, which develops a strongly associating regime up to the UCST. The uncertainties (error bars) are shown as 1 standard deviation.

the two-phase region (2-Φ), where the solution separates into coexisting liquid phases separated by a meniscus. The photos in Fig. 2 support the liquid–liquid phase separation of pAPAPS for select concentrations after equilibrating at 12 °C for 24 h with a polymer rich phase (lower, yellow phase) and a polymer poor phase (upper, colorless supernatant). A maximum in the cloud point temperature was observed and assigned as the critical temperature (T_c). Frequently, only a portion of the phase envelope was observed as a plateau,[6,8,15,21] but extending the concentration range as high as 300 mg/ml may reveal the characteristic UCST. Based upon estimates for the overlap concentration (c^*) using the radius of gyration (R_g), determined by SANS,[33] c^* = 82 mg/ml. The Flory theta temperature (Θ) for ideal solution behavior was estimated when A_2 = 0 as Θ ≈ 39 °C.[33] Therefore, pAPAPS chains, through thermodynamic interpretation, show poor solvent behavior below Θ and good solvent behavior above, with T_c ≈ 36 °C. Such UCST by cloud point was reported before in a molar mass series of polysulfobetaines;[24] however, the solvent quality (A_2) was not reported. Below Θ, under a poor solvent regime, attractions due to the large dipole moment of the zwitterionic propylsulfobetaine moiety (μ = 24 D in water[36]) could also influence the dynamics in the dilute and semi-dilute regimes. Such attractions, interpreted by solvent quality, are likely

FIG. 2. Photos showing liquid–liquid phase separation of pAPAPS at 12 °C in D_2O for several concentrations after equilibration at temperature for 24 h.

coupled to expected dipolar interactions that are not present in neutral polymers below their Θ temperatures. Computer simulations have been used to adjust the relative strengths of the interparticle potentials and dipolar contributions, which show a variety of morphological outcomes, even in dilute solutions.[37,38]

B. Temperature dependent dynamic light scattering

DLS was used to characterize the collective diffusion coefficient (D) within the 1-Φ region upon stepwise cooling and equilibration. An example of DLS autocorrelation functions at a scattering angle (θ) of 90° for pAPAPS at 8 mg/ml in D_2O is shown in Fig. 3(a). At high temperatures, only one mode is observed. However, upon cooling, a transition from one mode to two modes is observed with well-separated time constants (inverse decay rates). The measured intensity–intensity time correlation function, $G^{(2)}(q,\tau)$, is related to the normalized electric-field time correlation function, $g^{(1)}(q,\tau)$, by the Siegert relation,[39]

$$G^{(2)}(q,\tau) = A\left(1 + b\left|g^{(1)}(q,\tau)\right|^2\right), \tag{1}$$

where A is the average intensity-related baseline, and b is an instrument spatial coherence factor.[39] The baseline normalized correlation function, $G^{(2)}(q,\tau)/A - 1 = g^{(2)}(q,\tau) - 1$, is measured directly. In order to quantify these results, we determine the decay rates (Γ) of the auto-correlation functions by modeling the electric field correlation function $g^{(1)}(q,\tau)$ as a double exponential,

$$g^{(1)}(q,\tau) = A_f\left(e^{-\Gamma_f\tau}\right) + A_s\left(e^{-\Gamma_s\tau}\right) \tag{2}$$

to quantify the fast mode and slow mode contributions, where A_f and A_s are the amplitudes of the fast and slow modes, respectively, Γ_f and Γ_s are the decay rates of the fast and slow modes, respectively, and τ is the delay time. The intensity–intensity correlation function may be fit directly to determine the amplitudes and decay rates by assuming the Siegert relation and the form of $g^{(1)}(q,\tau)$. The diffusion coefficient was estimated from $D = \Gamma/q^2$, where q is the scattering vector defined by $q = (4\pi n/\lambda)\sin(\theta/2)$ and n is the solvent refractive index. When applicable, we estimate the hydrodynamic radius (R_h) from the Stokes–Einstein relation,

$$D = k_B\,T/6\pi\eta_o R_h, \tag{3}$$

where k_B is Boltzmann's constant, T is the temperature, and η_o is the viscosity of the solvent.

Two modes were first observed in a zwitterionic polycarboxybetaine of $M_w \approx 52\,000$ g/mol[14], with the fast mode reflecting the chain conformations and the slow mode attributed to interchain associates even under an extremely dilute solution of 4.65×10^{-5} g/ml. We also observe with pAPAPS that the fast mode is representative of the characteristic dimensions of single-chains, whereas the slow mode forms through the association of multiple polyzwitterion chains into dynamic clusters [Fig. 3(b)]. By examining the two-step decay in our correlation functions, the slow mode increases in amplitude (A_s) compared to the fast mode upon cooling. This qualitatively illustrates that the relative populations of multi-chain clusters and single chains are temperature dependent. The chain clustering becomes more prominent at lower temperatures near the phase boundary but above the cloud point while remaining in the one-phase region. In the example shown in Fig. 3(a), the two modes are observed for pAPAPS at 8 mg/ml in D_2O above the cloud point temperature of 14 °C.

After applying the Stokes–Einstein equation, Fig. 3(b) shows the estimated R_h values as a function of temperature for the fast and slow modes for the 8 mg/ml data. The R_g determined previously

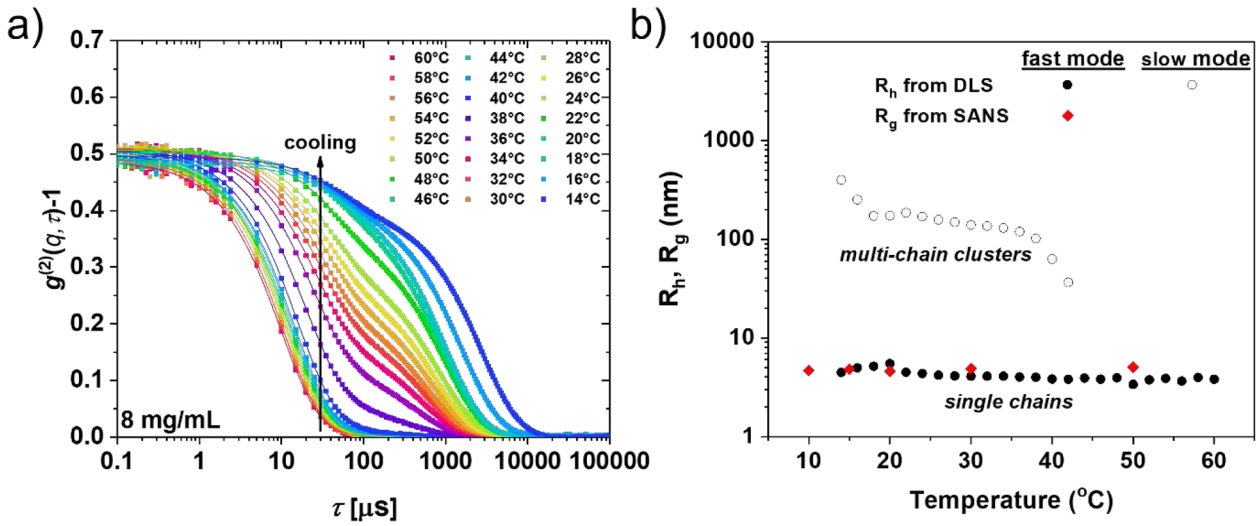

FIG. 3. (a) Temperature dependent intensity–intensity autocorrelation functions of pAPAPS (8 mg/ml) in D_2O at a scattering angle of 90°. The data are fitted to a double exponential, Eq. (2). (b) Hydrodynamic radius (R_h) of the fast mode (•) and slow mode (○) as a function of temperature at 8 mg/ml in D_2O and R_g (red diamond) determined at infinite dilution by SANS via Zimm plot analysis.[33]

from SANS are also shown as their extrapolated values to infinite dilution.[33] A qualitative comparison shows that the R_h from the fast mode represents the expected chain dimension for the pAPAPS when compared to the R_g and the value of R_g/R_h of ≈1.4, expected for flexible polymers. R_h was also independently determined by multi-angle DLS and analyzed by the double exponential model [Eq. (2)] and a REPES[40] analysis, which both returned similar results and were plotted in the supplementary material as Fig. S17. Therefore, we attribute the fast mode to single chains as related to the collective diffusion of mobile polyzwitterions.

C. Clustering temperature

We probe a little deeper into the distributions of fast mode and clustering within the 1-Φ region of the T-c phase boundary. The amplitudes of the two decay modes determined from fits to Eq. (2) may estimate the slow-mode cluster fraction (f_s) defined by $f_s = A_s/(A_f + A_s)$. The initial change in f_s upon cooling was used to estimate an onset temperature (T^*) where dynamic clusters start to emerge. Figure 4 summarizes the f_s as a function of temperature, between 4 and 20 mg/ml, in which f_s increases with decreasing temperature. This behavior is consistent with a shift in equilibrium from predominantly single chains (unimers) at high temperatures and a broad transition to multi-chain clustering defined by T^*. However, we note that the double exponential analysis of the autocorrelation functions identifies an amplitude for the slow mode that does not completely go away at temperatures up to 60 °C. A closer look at the autocorrelation functions reveals that the slow mode at concentrations less than 20 mg/ml is negligible and possibly even in the baseline noise of the data; a REPES analysis supports this (Fig. S16). Therefore, the T^* is only plotted up to 20 mg/ml because above this concentration we observe a persistent slow mode even at higher temperatures (Fig. S15), which suggests observable populations with larger size distributions of pAPAPS (Fig. S16). We have determined that at these higher concentrations (≥36 mg/ml), a simple assessment of unimers and clusters by DLS is not possible, and T^* could not be defined in the temperature range probed (up to 60 °C).

The appearance of a slow mode as the temperature decreases points toward a dynamic exchange of single chains and reversible clusters of chains. We performed a temperature cycle experiment at 8 mg/ml to probe the reversibility. Figure 5 shows the population distributions of the unimers and clusters at various temperatures from a REPES analysis applied to the Stokes–Einstein equation. After equilibrating at an initial temperature of 50 °C for 2 h, only a unimer population is observed. This unimer population remains relatively constant in peak R_h value and distribution between 50 and

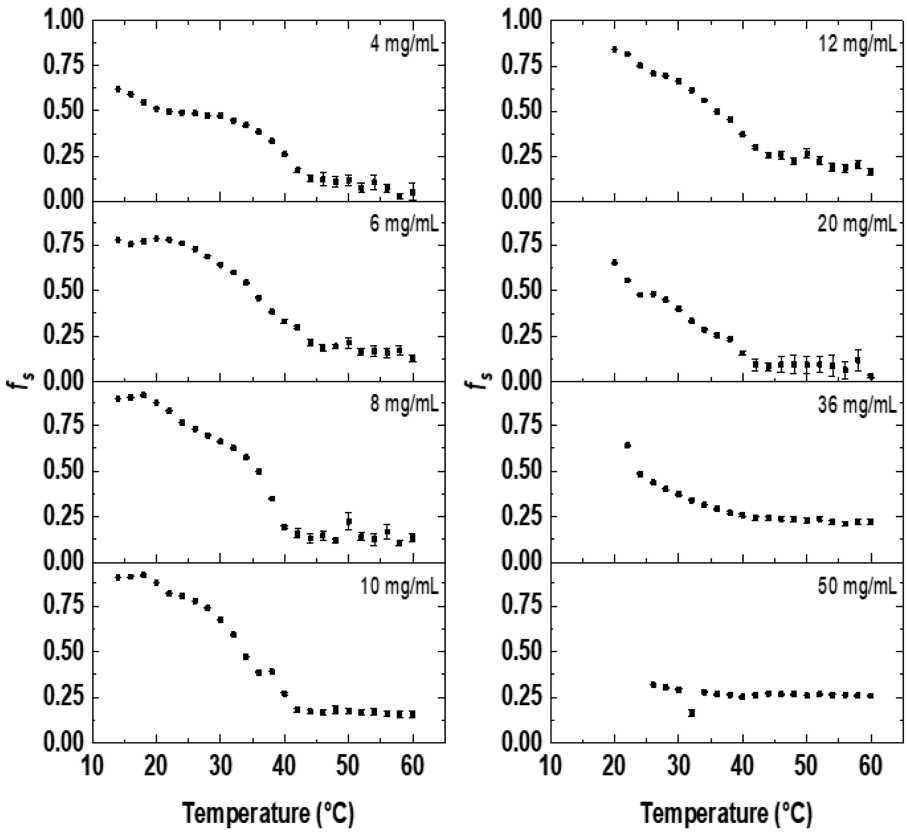

FIG. 4. f_s as a function of temperature for pAPAPS in D_2O at different concentrations determined by DLS at a scattering angle of 90°. The uncertainties (error bars) are shown as 1 standard deviation.

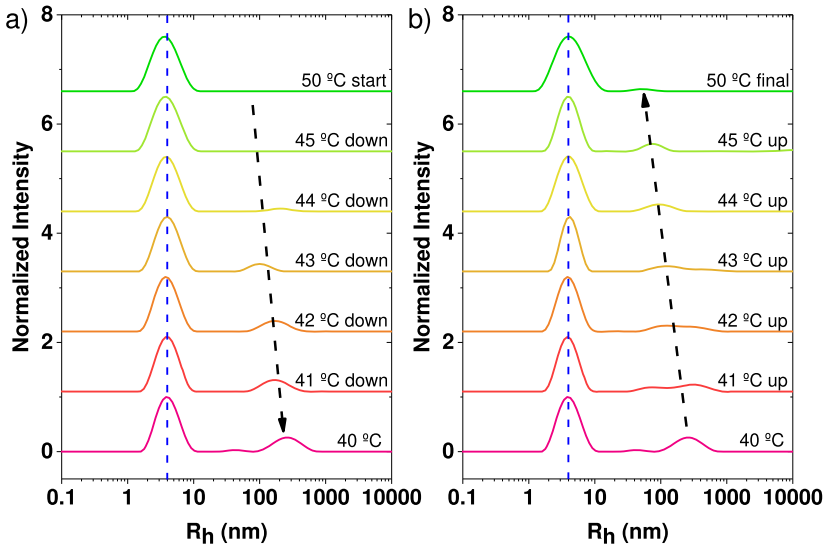

FIG. 5. Temperature dependent size distributions of unimers and aggregates determined from DLS of pAPAPS at 8 mg/ml in D_2O at a scattering angle of 90°: (a) temperature ramped down from a start point of 50–40 °C; (b) temperature ramped up from 40 °C to a final temperature of 50 °C. The temperature was adjusted using a ramp rate of 5 °C/min, and the sample was allowed to equilibrate at each temperature for 5 min before the data were collected over 15 min. The dashed arrow highlights the emergence and disappearance of the slow mode as the temperature changes.

40 °C as the temperature is incrementally lowered. However, the slow mode appears at 44 °C and shifts toward larger sizes upon cooling [Fig. 5(a)]. This onset of interpolymer associative interactions, followed by an increase in size and relative amplitude (f_s), qualitatively shows a shift from unimer to dynamic clusters. Upon heating from 40 to 50 °C, the polydisperse cluster population shifts toward smaller sizes and decreases in amplitude, suggesting the dissociation of chains [Fig. 5(b)]. Noteworthy, a slight hysteresis appears where, upon heating to 50 °C, a small amplitude of clustering remains. This apparent difference may resemble ultra-long relaxation times for chains from interpolymer interactions, in which higher temperatures (driving force) and longer equilibration (kinetics) are required.

D. Polyzwitterion dynamics coupled to phase separation

The UCST of pAPAPS exhibits an apparent critical polymer concentration (c_c) of ≈65 mg/ml and a critical temperature (T_c) of ≈36 °C. When T^* is shown on the same plot as the cloud points [Fig. 1(c)], a regime of multi-chain clustering exists at $T < T^*$ and predominantly one mode at $T > T^*$. T^* minimally changes from 40 to 43 °C as c increases from 4 to 20 mg/ml, respectively. The temperature gap between the cloud points and T^* is ~33 °C at 4 mg/ml and narrows to about 24 °C at 20 mg/ml. This relationship of the soluble multi-chain clusters emerging at T^* close to the poor solvent domain $T < \Theta$ prior to the cloud points was not previously reported. Therefore, these trends need to be validated as a function of molar mass and different zwitterionic moieties (carboxybetaine, sulphobetaines, and phosphobetaines, for example) to generalize these observations. The behavior appears similar to an expected gelation line that extends from low to high polymer concentrations with a positive slope, as predicted in polymers with associative interactions, such as telechelic polymers,[41] polyampholytes,[42] and hydrogen bonding systems. However, T^* occurs well below c^* and the proximity with Θ is surely not a coincidence. We speculate that the poor-solvent regime provides an underlying driving-force for the increase in finite-sized dynamic clusters. However, since dipolar interactions are short-ranged, the zwitterionic moiety attractions may be modeled through an effective Flory–Huggins interaction parameter (χ) with UCST behavior, while the dipolar attraction gives rise to the soluble polydisperse clusters on the 100–1000 nm scale. Such arguments have been theoretically suggested with dipolar attraction origins.[32]

E. Concentration dependence of the fast mode

We attribute the fast mode to the collective diffusion coefficient of the polymer solution. The concentration dependence of the collective diffusion coefficient, D,[43–45] can be expressed by a virial expansion as

$$D = D_0\left[1 + k_d c + k_{d2} c^2 + \cdots\right] \quad (4)$$

with the diffusion coefficient at infinite dilution (D_o) and the dynamic virial coefficients k_d and k_{d2}.[43–45] Theoretical interpretations of these virial coefficients for spherical particle suspensions with short-range repulsive interactions, sticky attractive interactions, and polymers in good, theta, and poor solvents are available.[46] Quantitative comparisons require precision measurements of the molar mass dependence, viscosity, and second virial coefficient. Such a complete evaluation is not possible here, but we compare the concentration dependence of the fast mode in terms of the col-

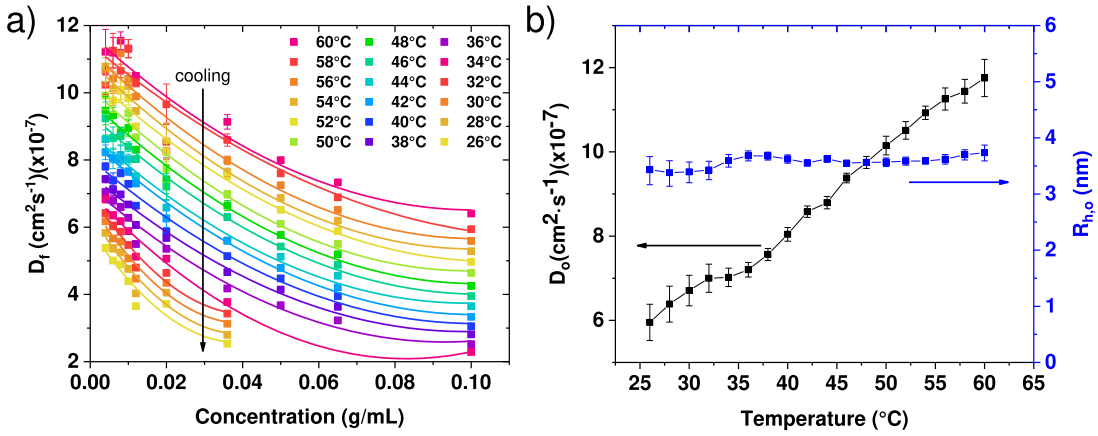

FIG. 6. (a) Concentration dependent diffusion coefficient (D_f) of the fast mode of pAPAPS in D_2O solutions for various temperatures from scattering at 90°. (b) Left axis $D_{f,0}$ and right axis application of the Stokes–Einstein equation showing the temperature dependent $R_{h,0}$. The uncertainties (error bars) are shown as 1 standard deviation of the fit to Eq. (4).

lective diffusion coefficient formalism and speculate on the trends with respect to the expected attractive dipolar interactions between polyzwitterions for the relatively low molar mass chains below and near c^*.

Plotting D_f vs c shows a virial expansion relationship, with systematic deviations from linearity when analyzed from 4 to 100 mg/ml [Fig. 6(a)]. At a fixed T, D_f decreases as the concentration increases. However, there is a strong temperature dependence on D_f, in which the diffusion of polymer chains reduces with decreasing temperature. We find that applying Eq. (4) with the virial coefficients[29] k_d and k_{d2} fits the entire c and T trends as the overlap concentration is approached ($c^* \approx 82$ mg/ml). Figure 6(a) shows the concentration dependence of D_f at various temperatures with fits to Eq. (4) at all temperatures and as c/c^* approaches unity. The diffusion coefficient extrapolated to infinite dilution, D_0, also decreases with decreasing temperature [Fig. 6(b)]. Applying the Stokes–Einstein relationship with the known temperature dependence of the solvent zero-shear viscosity, D_0 simply reflects the diffusion of the polyzwitterion chain with hydrodynamic radius at infinite dilution ($R_{h,o}$), as shown in Fig. 6(b). The $R_{h,o}$ data show a slight variation between ~35 and 40 °C, near the Θ temperature, and could reveal fluctuations and non-uniformity in coil size in the Θ-region due to intra-polymer dipole–dipole attractions that weaken with increasing temperature. The concentration ($c < c^*$) and temperature dependence ($T < T^*$ or $T > T^*$) of the collective diffusion coefficient, as quantified by Eq. (4), are strongly influenced by the interpolymer interactions as temperature decreases to T^* and below Θ. D_f is estimated and analyzed in the 1-Φ region, not within the 2-Φ region where the kinetics of phase separation take place.

The k_d value provides insight into two-body interactions that influence the diffusion coefficient.[29] For pAPAPS, the value of k_d is negative and slightly decreases with decreasing temperature down to 38 °C, below which k_d decreases rapidly (Fig. 7). The significance of these negative k_d values (Table S1) is a strengthening of concentration dependent behavior of pAPAPS. Interestingly, the change in scaling of k_d coincides with a transition into poor solvent conditions (Θ ≈ 39 °C),[33] in which the slow mode becomes significant [for example, as observed at 8 mg/ml in Fig. 3(a)]. This trend in k_d can also be described by the expected interchain interactions of the polyzwitterion that would influence the concentration dependent diffusion in the presence of larger structures. However, plotting k_d vs temperature does not sufficiently describe the temperature dependent scaling of the interpolymer interactions. It is known that k_d is related to the hydrodynamic and second virial osmotic coefficients[29] as $k_d = 2A_2M_w - k_s$, in which M_w is the mass-average relative molar mass of the polymer and k_s is the virial coefficient that describes the concentration dependence of the friction coefficient, which is unknown and no doubt dependent on A_2M_w.

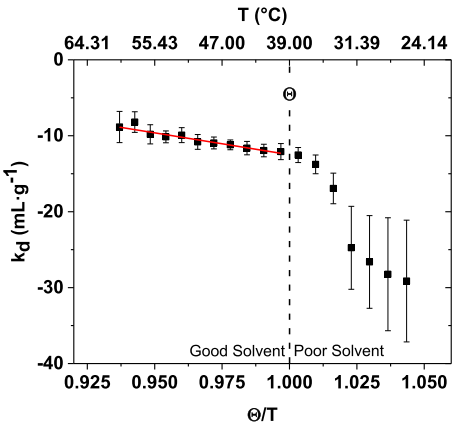

FIG. 7. Concentration virial coefficient (k_d) vs Θ/T (from the K scale) for pAPAPS in D_2O without salt. The solid line is a fit to Eq. (5). The vertical dashed line highlights the separation between thermodynamically good (Θ/T < 1) and poor (Θ/T > 1) solvent regimes. The top axis shows k_d vs T. The uncertainties (error bars) are shown as 1 standard deviation.

Within the mean field Flory–Huggins theory, near the Θ point $A_2 \approx \left(\frac{1}{2} - \chi\right)$,[45,47] where χ is the Flory–Huggins polymer–solvent interaction parameter. The interaction parameter is phenomenologically expressed as $\chi = \frac{\alpha}{T} + \beta$, where α and β are the parameters describing the enthalpy and entropy contributions to interactions, respectively.[45,48] The β is not a result of the Flory–Huggins theory but is often included to fit experimental data as well as the concentration dependence of χ. After substitution for A_2, an inverse temperature relationship for k_d is predicted by Eq. (5), in which B is the constant that combines M_w, β, and k_s effects, leading to $B = M_w - 2M_w\beta - k_s$,

$$k_d = -\frac{2\alpha M_w}{T} + B. \tag{5}$$

Figure 7 shows the linear fit of k_d plotted vs Θ/T (red solid line) under good solvent conditions, agreeing with the mean field relationship relative to Θ, in which good ($\Theta/T < 1$) and poor ($\Theta/T > 1$) solvent regimes are highlighted by the dashed line. At temperatures below Θ (poor solvent), k_d deviates from the inverse temperature dependence, suggesting additional contributions that influence the diffusion of the fast mode under poor solvent conditions. However, evaluating the temperature dependence of the interaction parameter by SAXS or SANS would provide a better account of the relative thermodynamic contributions or separation of a polymer–solvent interaction parameter from the dipole–dipole contributions that serve to increase the effective hydrophobicity.[49]

At high temperatures and infinite dilution (D_0), the pAPAPS molecules diffuse as individual chains; however, in dilute solutions and as the temperature decreases, multi-chain dynamic clusters form with a separation of diffusional timescales, as shown in the autocorrelation functions. Such dynamics represent chains that diffuse in the presence of larger clusters. Assuming that the temperature dependence of the solution viscosity is partly responsible for the decrease in the diffusion coefficient at lower temperatures, a larger contributor is the size and interaction with interpolymer clusters. The decrease in the diffusion coefficient of the fast mode at finite polymer concentrations as temperature decreases is attributed to the collective diffusion and attractive interpolymer interactions with the clusters, thus reducing the mobility throughout the solution. Under the poor solvent regime, the interactions are attractive, which partly explains the deviation in k_d from the well-defined inverse temperature scaling. We speculate that as more clusters form, this perturbed diffusive mode becomes more prevalent. In addition, as such, we see a larger decrease in k_d with temperature below Θ, where clustering becomes predominant (Fig. 7). In addition, possible is a shift in the diffusive mode from chains diffusing freely to exchanging between the clusters and bulk solution due to the change in the solvent quality. This likely occurs to some extent under more concentrated solution conditions, in which chain exchange would be more prevalent. The k_{d2} term from Eq. (4) shows positive values (tabulated in Table S1), thereby possibly reflecting an additional compensating interaction such as the third virial osmotic coefficient (A_3), where $k_{d2} = 3A_3M_w - k_{s2} - k_dk_s$, in which k_{s2} is the sedimentation coefficient tied to three-body interactions or a concentration dependence of the friction coefficient from the more well-defined k_d.[29] This is further demonstrated at lower temperatures, where the cluster population increases, indicating that single chains are being incorporated into existing larger structures or coalescing into new ones. This is not surprising since at lower temperatures pAPAPS will transition to poor solvent conditions and prefer polymer–polymer interactions over polymer–solvent interactions; hence the observed shift in scaling of k_d and k_{d2} below the Θ of pAPAPS.

F. Slow mode observations

We now shift our attention to the slow mode, which exhibits more complex behavior depending on the concentration regime probed. For simplicity, we show the slow mode at 50, 38, and 34 °C to capture the concentration dependent diffusion in both good, theta, and poor solvent conditions (Fig. 8). At 50 °C, D_s exhibits a decreasing trend with increasing concentrations from 36 to 100 mg/ml. This trend is attributed to an increase in the size of the diffusing multi-chain clusters. Importantly, 50 °C is above T^* for concentrations of 20 mg/ml and below; therefore, no D_s data are shown in this region. However, when pAPAPS is in poor solvent conditions at 34 °C, the concentration dependent behavior of the slow mode changes depending on the concentration range. From 4 to 20 mg/ml at 34 °C, D_s decreases with increasing concentration. As the concentration regime increases, D_s is now observed to increase from 36 to 100 mg/ml in poor solvent conditions. Noteworthy, at 38 °C (near Θ), D_s seems to be less concentration dependent, highlighting a midpoint or transition between the diffusive behavior of the slow mode between good and poor solvent. The structure of the clusters, however, requires an appropriate technique. Langevin dynamics simulations observe a variety of structures that depend on the distance between zwitterionic units along the main chain, such that closer-spaced zwitterion groups lead to the formation of micellar and vesicle structures.[38]

G. Salt reduces the dipolar attractions in pAPAPS

As added evidence that the multi-chain clusters are formed by dipolar attractions, we find that with 100 mM NaCl salt, the slow

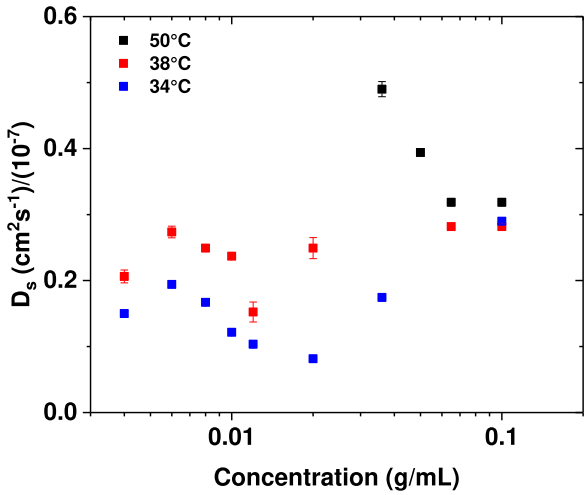

FIG. 8. Concentration dependent diffusion coefficients of the slow mode (D_s) of pAPAPS at 50, 38, and 34 °C in D_2O. The uncertainties (error bars) are shown as 1 standard deviation.

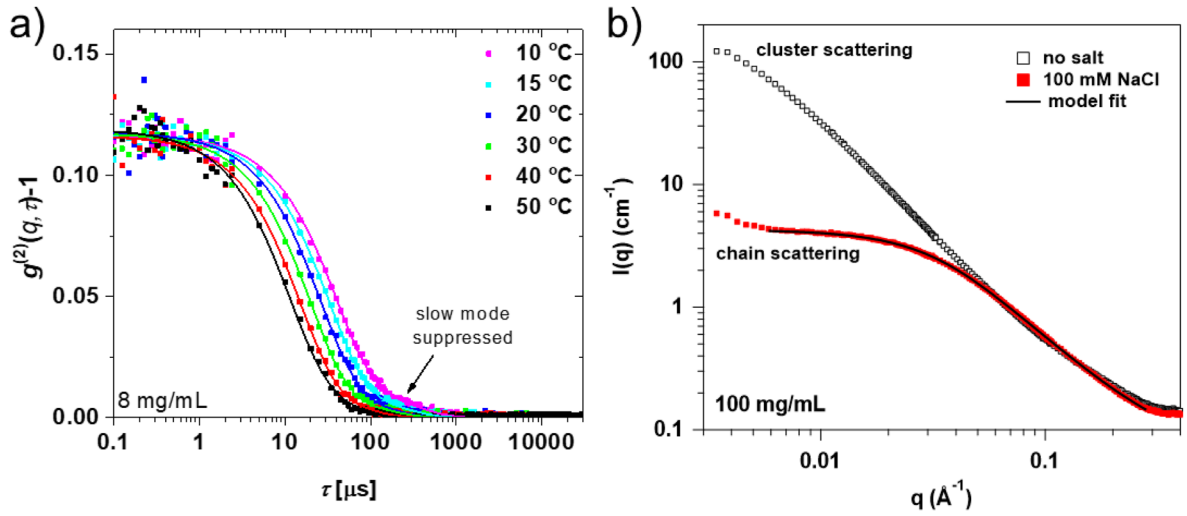

FIG. 9. (a) Temperature dependent intensity–intensity autocorrelation functions of pAPAPS (8 mg/ml) in 100 mM NaCl in D_2O at a scattering angle of 90°. The data are fitted to a double exponential, Eq. (2). (b) SANS of pAPAPS (100 mg/ml) in D_2O and 100 mM NaCl in D_2O at 50 °C. The model fit to the polymer with an excluded volume form factor estimates the R_g of (4.32 ± 0.01) nm, where the uncertainty (±) represents one standard deviation from the fit.

mode that represents larger clusters is suppressed in the autocorrelation function, even down to 10 °C, when compared to no salt (Fig. 9). In addition, the R_h values agree with expected single chains (Fig. S17). To note, the UCST is lowered by the addition of salt and does not appear above the freezing point. Finally, in the absence of the attractions and the suppression of the slow mode, the solvent quality remains good with $A_2 > 0$ at all temperatures.[33] These observations support the idea that the slow mode and the dipolar interactions are related to the poor solvent conditions at low temperatures. Furthermore, extending the q-range of SANS using static light scattering at 8 mg/ml in D_2O at 50 °C shows primarily chain scattering (Fig. S22), indicating elevated temperatures lead to reduced multi-chain clusters.

At high concentrations, SANS of pAPAPS at 100 mg/ml and at 50 °C shows scattering of clusters in the absence of salt [Fig. 9(b)]. Recall that a slow mode was observed even at high temperatures in semidilute solutions (Fig. 8). The low-q scattering can be modeled by the Ornstein–Zernike equation (Fig. S23) to estimate the correlation length (ξ) of the fluctuation or cluster size ξ = (22.5 ± 0.2) nm that far exceeds single chain dimensions. Upon the addition of 100 mM NaCl, the scattering in Fig. 9(b) changes substantially at the same polymer concentration and appears similar to chain scattering. In order to quantify this high-salt data, the phenomenological model of a polymer with an excluded volume form factor was fitted to the SANS data without any structure factor contribution.[50] This phenomenological model was not developed for charged polymers or polyzwitterions but can be applied to estimate the R_g and the high-q limiting law scaling of the excluded volume exponent (ν). As described by Hammouda[50] and Igor Pro Analysis routines,[35] ν is the inverse of the Porod exponent, where ν is ~3/5 for swollen chains in a good solvent, 1/2 for ideal Gaussian chains under theta solvent conditions, and 1/3 for globules. The fit estimates R_g = (4.32 ± 0.01) nm and ν = 0.564 ± 0.001, with additional details in the supplementary material (Fig. S24). The R_g is slightly smaller than the infinite dilution values[33] of (5.05 ± 0.12) nm at the same salt concentration and temperature. This was expected since, above c^* and in the semidilute regime, the short-range excluded volume interactions are screened, leading to a characteristic concentration dependence of the chain dimensions.[20] This is only an estimate for chain dimensions since this was not a high concentration deuterium labeled chain experiment[51] and the polymer excluded volume form factor model does not consider inter-chain interactions. The value of ν = 0.564 is very close to self-avoiding walk chain statistics (good solvent) and compares to the average value of ν = 0.588 (where ν = 1/Porod exponent) from dilute solution.[33] The substantial change in static scattering with the addition of salt supports the reduced dipole–dipole interactions with reasonable estimates for R_g and ν. Additional measurements utilizing SANS and SAXS combined with a physics-based model are necessary to refine these observations in terms of the temperature-dependence of the static correlation length and the separation of dipolar attractions from an interaction parameter.

IV. CONCLUSIONS

A model polysulfobetaine, poly(3-(acrylamidopropyl-dimethyl-ammonium) propyl-1-sulfonate), was studied by DLS as a function of temperature and concentration. The temperature-concentration cloud point diagram shows UCST behavior with a clustering temperature characterized by the reversible appearance and disappearance of a slow mode between 4 and 20 mg/ml. A temperature gap between the cloud point temperature and T^* observes the slow mode of multi-chain dynamic clusters. The relative amount of slow mode was dependent upon the distance below the Θ temperature, or T^* and c/c^*. The population distributions of the fast mode and slow mode clusters are reversible with a

hysteresis upon heating. Having identified the two dynamics modes, the temperature and concentration dependent diffusion coefficients of the fast mode represent a collective diffusion of polyzwitterion chains with a negative k_d. The negative sign and magnitude of k_d at T > Θ are not indicative of good solvent behavior, even though $A_2 > 0$. However, the negative value of k_d is consistent with numerous measurements and the dynamics of neutral polymer solutions at the Θ point. The present measurements are not within the asymptotic semi-dilute regime, where positive k_d values are expected under good solvent conditions, as shown by Zhang *et al.*[52] for polystyrene in toluene. The additional dynamic positive virial term k_{d2} was included to fit the fast collective diffusion as c^* approached. The collective dynamics of the fast mode are not adequately described by the available neutral polymer theoretical framework based on osmotic compressibility arguments due to the influence of the slow mode. However, k_d follows an inverse temperature dependence above Θ, with strong negative deviations below Θ when the slow mode becomes prominent. In such cases, the interpretation of k_d in the presence of dynamic clustering cannot be simply forced into a particular form based on the available framework from neutral polymer solutions. We conclude that the fast mode collective diffusion of polyzwitterion chains in the presence of slow-moving clusters leads to a strongly perturbed diffusion environment at $T < T^*$ and $c < c^*$, i.e., before overlapping chains within the semi-dilute regime. These short-range attractive interactions between chains and stable, multi-chain clusters are hypothesized to arise from inter-chain dipolar interactions at lower temperatures and finite concentrations. In addition, as such, the slowing of the fast mode upon the emergence of the slow mode supports that dipolar attractive interactions induce the onset of multi-chain clusters below Θ that precede and couple to the increase in concentration fluctuations as the UCST is approached. Similar trends and phase diagrams of other polyzwitterions would need to be verified in order to determine universal scaling laws regarding slow and fast mode behavior.

We speculate that interpretations of the collective diffusion behavior need to consider a source of attraction based on the dipolar interactions, known for isolated chains, but also the inter-molecular interactions that lead to the finite-sized multi-chain clusters. While the slow mode in polyzwitterions was observed by numerous groups on different systems, the present study identifies how a change from good to poor solvent behavior within the 1-Φ region controls the multi-chain cluster population. The concentration range studied below c^* reflects an expected system with large concentration fluctuations, and as observed, the increase in slow mode amplitude as the temperature is lowered or concentration is increased suggests such an increase in concentration fluctuations as the system moves toward phase separation. The present study provides insight into the dynamics of polyzwitterion solutions near the phase boundary, but refined measurements such as SAXS and SANS are needed to develop a more quantitative analysis of the interactions in semidilute solutions of polyzwitterions. Preliminary SANS at high temperatures in the absence of salt shows scattering by clusters and, therefore, highly interacting chains, consistent with the observation of slow mode in DLS. The addition of salt substantially affects the static scattering, revealing chain scattering as modeled by a polymer with an excluded volume form factor. Such experiments within the semidilute regime at 100 mg/ml and above the UCST support how salt modulates the strong inter-chain dipole–dipole attractions.

SUPPLEMENTARY MATERIAL

The supplementary material includes the following data: synthetic details and characterization of monomer, CTA, and polymer; multi-angle and 90° DLS autocorrelation functions; temperature dependent gamma vs q^2 plots from multi-angle DLS; temperature dependent size distributions from 90° DLS determined from REPES analysis; temperature and concentration dependent hydrodynamic radii of fast and slow modes; a table of the fitting parameters of Eq. (4); concentration dependent diffusion coefficient of the slow mode at all temperatures probed; ^{1}H-NMR of pAPAPS when initially dissolved in D_2O vs after a temperature ramp cycle and sitting in D_2O for 2 weeks to show the absence of hydrolysis of the zwitterion moiety during the experiments; and 90° $g^{(1)}(q,\tau)$ autocorrelation functions of pAPAPS at 8 mg/ml for various temperatures in D_2O and 100 mM NaCl in D_2O. Ornstein–Zernike analysis and polymer excluded volume model fits. Combined static light scattering and small-angle neutron scattering data for 8 mg/ml in D_2O at 50 °C.

Note added in proof. Certain equipment, instruments, software, or materials are identified in this paper in order to adequately specify the experimental procedure. Such identification is not intended to imply the recommendation or endorsement of any product or service by NIST, nor is it intended to imply that the materials or equipment identified are necessarily the best available for the purpose.

The symbols M and mM are used to represent mol/l and mmol/l, respectively, and are not in SI units but are used to adhere to the conventions of the journal as well as the symbol l in place of L for liter.

ACKNOWLEDGMENTS

P.D.P. acknowledges partial support from the National Institute of Standards and Technology (NIST)-National Research Council Research Associates Program. Y.M., P.D.P., and V.M.P. acknowledge partial support from the NIST Materials Genome Initiative. We thank Jack Douglas (NIST) for helpful discussions and Yimin Mao (NIST) for assistance with SANS measurements.

AUTHOR DECLARATIONS

Conflict of Interest

The authors have no conflicts to disclose.

Author Contributions

Phillip D. Pickett: Conceptualization (equal); Investigation (lead); Writing – original draft (equal); Writing – review & editing (equal). **Yuanchi Ma**: Conceptualization (equal); Investigation (supporting); Writing – original draft (supporting); Writing – review & editing (equal). **Vivek M. Prabhu**: Conceptualization (equal); Investiga-

tion (supporting); Resources (lead); Supervision (lead); Writing – original draft (supporting); Writing – review & editing (equal).

DATA AVAILABILITY

The primary data that support the findings of this study are available within the article; The data that support the findings of this study are available from the corresponding author upon reasonable request.

REFERENCES

[1]L. Zheng, H. S. Sundaram, Z. Wei, C. Li, and Z. Yuan, "Applications of zwitterionic polymers," React. Funct. Polym. **118**, 51–61 (2017).

[2]J. Du, Y. Tang, A. L. Lewis, and S. P. Armes, "pH-sensitive vesicles based on a biocompatible zwitterionic diblock copolymer," J. Am. Chem. Soc. **127**, 17982–17983 (2005).

[3]N. M. Nizardo, D. Schanzenbach, E. Schönemann, and A. Laschewsky, "Exploring poly(ethylene glycol)-polyzwitterion diblock copolymers as biocompatible smart macrosurfactants featuring UCST-phase behavior in normal saline solution," Polymers **10**, 325 (2018).

[4]Q. Shao and S. Jiang, "Molecular understanding and design of zwitterionic materials," Adv. Mater. **27**(1), 15–26 (2015).

[5]S. Kudaibergenov, W. Jaeger, and A. Laschewsky, "Polymeric betaines: Synthesis, characterization, and application," in *Supramolecular Polymers Polymeric Betains Oligomers*, Advances in Polymer Science series (Springer, Berlin, Heidelberg, 2006), Vol. 201, pp. 157–224.

[6]Y. Zhu, J. M. Noy, A. B. Lowe, and P. J. Roth, "The synthesis and aqueous solution properties of sulfobutylbetaine (co)polymers: Comparison of synthetic routes and tuneable upper critical solution temperatures," Polym. Chem. **6**, 5705–5718 (2015).

[7]A. B. Lowe and C. L. McCormick, "Synthesis and solution properties of zwitterionic polymers," Chem. Rev. **102**, 4177–4190 (2002).

[8]V. Hildebrand, A. Laschewsky, M. Päch, P. Müller-Buschbaum, and C. M. Papadakis, "Effect of the zwitterion structure on the thermo-responsive behaviour of poly(sulfobetaine methacrylates)," Polym. Chem. **8**, 310–322 (2017).

[9]P. A. Woodfield, Y. Zhu, Y. Pei, and P. J. Roth, "Hydrophobically modified sulfobetaine copolymers with tunable aqueous UCST through postpolymerization modification of poly(pentafluorophenyl acrylate)," Macromolecules **47**, 750–762 (2014).

[10]J. Niskanen and H. Tenhu, "How to manipulate the upper critical solution temperature (UCST)?," Polym. Chem. **8**(1), 220–232 (2017).

[11]E. E. Kathmann, L. A. White, and L. McCormick, "Water soluble polymers: 70. Effects of methylene vs propylene spacers in the pH and electrolyte responsiveness of zwitterionic copolymers incorporating carboxybetaine monomer," Polymer **38**, 879–886 (1997).

[12]R. S. Armentrout and C. L. McCormick, "Water soluble polymers. 76. Electrolyte responsive cyclocopolymers with sulfobetaine units exhibiting polyelectrolyte or polyampholyte behavior in aqueous media," Macromolecules **33**, 419–424 (2000).

[13]J. D. Delgado and J. B. Schlenoff, "Static and dynamic solution behavior of a polyzwitterion using a Hofmeister salt series," Macromolecules **50**, 4454–4464 (2017).

[14]A. Niu, D.-J. Liaw, H.-C. Sang, and C. Wu, "Light-scattering study of a zwitterionic polycarboxybetaine in aqueous solution," Macromolecules **33**(9), 3492–3494 (2000).

[15]F. Wang, J. Yang, and J. Zhao, "Understanding anti-polyelectrolyte behavior of a well-defined polyzwitterion at the single-chain level," Polym. Int. **64**, 999–1005 (2015).

[16]D. N. Schulz, D. G. Peiffer, P. K. Agarwal, J. Larabee, J. J. Kaladas, L. Soni, B. Handwerker, and R. T. Garner, "Phase behaviour and solution properties of sulphobetaine polymers," Polymer **27**(11), 1734–1742 (1986).

[17]J. Yu, Z. Li, X. Liu, S. Song, G. Gao, Q. Zhang, and F. Liu, "Molecular size and morphology of single chains of poly(sulfobetaine methacrylate)," Chem. Res. Chin. Univ. **32**, 499–504 (2016).

[18]R. Kumar and G. H. Fredrickson, "Theory of polyzwitterion conformations," J. Chem. Phys. **131**(10), 104901 (2009).

[19]M. Beer, M. Schmidt, and M. Muthukumar, "The electrostatic expansion of linear polyelectrolytes: Effects of gegenions, Co-ions, and hydrophobicity," Macromolecules **30**(26), 8375–8385 (1997).

[20]M. Muthukumar, "50th anniversary perspective: A perspective on polyelectrolyte solutions," Macromolecules **50**(24), 9528–9560 (2017).

[21]V. Hildebrand, A. Laschewsky, and E. Wischerhoff, "Modulating the solubility of zwitterionic poly((3-methacrylamidopropyl)ammonioalkane sulfonate)s in water and aqueous salt solutions via the spacer group separating the cationic and the anionic moieties," Polym. Chem. **7**, 731–740 (2016).

[22]V. Hildebrand, A. Laschewsky, and D. Zehm, "On the hydrophilicity of polyzwitterion poly (*N*,*N*-dimethyl-*N*-(3-(methacrylamido)propyl)ammoniopropane sulfonate) in water, deuterated water, and aqueous salt solutions," J. Biomater. Sci., Polym. Ed. **25**, 1602–1618 (2014).

[23]M. B. Huglin and M. A. Radwan, "Unperturbed dimensions of a zwitterionic polymethacrylate," Polym. Int. **26**(2), 97–104 (1991).

[24]P. Mary, D. D. Bendejacq, M. P. Labeau, and P. Dupuis, "Reconciling low- and high-salt solution behavior of sulfobetaine polyzwitterions," J. Phys. Chem. B **111**, 7767–7777 (2007).

[25]Z. Cao and G. Zhang, "Dynamics of polyzwitterions in salt-free and salt solutions," Phys. Chem. Chem. Phys. **17**, 27045–27051 (2015).

[26]D. W. Schaefer and C. C. Han, "Quasielastic light scattering from dilute and semidilute polymer solutions," in *Dynamic Light Scattering, Applications of Photon Correlation Spectroscopy*, edited by R. Pecora (Plenum Press, New York, 1985), Chap. 5, pp. 181–243.

[27]P. M. Cotts and J. C. Selser, "Polymer-polymer interactions in dilute solution," Macromolecules **23**(7), 2050–2057 (1990).

[28]L. J. Fetters, N. Hadjichristidis, J. S. Lindner, and J. W. Mays, "Molecular weight dependence of hydrodynamic and thermodynamic properties for well-defined linear polymers in solution," J. Phys. Chem. Ref. Data **23**(4), 619–640 (1994).

[29]Y. Tsunashima, T. Hashimoto, and T. Nakano, "First and second concentration-dependent coefficients of translational diffusion and sedimentation for poly (α-methylstyrene) in a good solvent," Macromolecules **29**, 3475–3484 (1996).

[30]M. Muthukumar, "Ordinary-extraordinary transition in dynamics of solutions of charged macromolecules," Proc. Natl. Acad. Sci. U. S. A. **113**(45), 12627–12632 (2016).

[31]S. Morozova, G. Hu, T. Emrick, and M. Muthukumar, "Influence of dipole orientation on solution properties of polyzwitterions," ACS Macro Lett. **5**(1), 118–122 (2016).

[32]D. Jia and M. Muthukumar, "Dipole-driven interlude of mesomorphism in polyelectrolyte solutions," Proc. Natl. Acad. Sci. U. S. A. **119**(40), e2204163119 (2022).

[33]P. D. Pickett, Y. Ma, M. Lueckheide, Y. Mao, and V. M. Prabhu, "Temperature dependent single-chain structure of poly[3-(acrylamidopropyl-dimethyl-ammonium) propyl-1-sulfonate] via small-angle neutron scattering," J. Chem. Phys. **156**, 214904 (2022).

[34]P. D. Pickett, C. R. Kasprzak, D. T. Siefker, B. A. Abel, M. A. Dearborn, and C. L. McCormick, "Amphoteric, sulfonamide-functionalized 'polysoaps': CO_2-induced phase separation for water remediation," Macromolecules **51**, 9052–9059 (2018).

[35]S. Kline, "Reduction and analysis of SANS and USANS data using IGOR Pro," J. Appl. Crystallogr. **39**(6), 895–900 (2006).

[36]M. Galin, A. Chapoton, and J.-C. Galin, "Dielectric increments, intercharge distances and conformation of quaternary ammonioalkylsulfonates and alkoxydicyanoethenolates in aqueous and tirfluoroethanol solutions," J. Chem. Soc., Perkin Trans. 2 **2**(3), 545–553 (1993).

[37]K. Van Workum and J. F. Douglas, "Symmetry, equivalence, and molecular self-assembly," Phys. Rev. E **73**(3), 031502 (2006).

[38]J. P. Mahalik and M. Muthukumar, "Simulation of self-assembly of polyzwitterions into vesicles," J. Chem. Phys. **145**(7), 074907 (2016).

[39]G. Fytas, *Scattering: Scattering and Inverse Scattering in Pure and Applied Science* (Academic Press, San Diego, CA, 2003), pp. 849–863.
[40]W. Brown, *Dynamic Light Scattering: The Method and Some Applications* (Oxford University Press, New York, 1993).
[41]F. Tanaka, "Theory of thermoreversible gelation," Macromolecules **22**(4), 1988–1994 (1989).
[42]S. Das and M. Muthukumar, "Microstructural organization in α-synuclein solutions," Macromolecules **55**(11), 4228–4236 (2022).
[43]H. Yamakawa, *Modern Theory of Polymer Solutions* (Harper & Row, Publishers, Inc., 1971).
[44]C. C. Han and A. Z. Akcasu, "Concentration dependence of diffusion coefficient at various molecular weights and temperatures," Polymer **22**, 1165–1168 (1981).
[45]P. C. Hiemenz and T. P. Lodge, *Polymer Chemistry*, 2nd ed. (Taylor & Francis, 2007).
[46]A. L. Kholodenko and J. F. Douglas, "Generalized Stokes-Einstein equation for spherical particle suspensions," Phys. Rev. E **51**(2), 1081–1090 (1995).
[47]M. Muthukumar and S. F. Edwards, "Chain statistics and scaling concepts," Compr. Polym. Sci. Suppl. **2**, 1–47 (1989).
[48]P. Knychała, K. Timachova, M. Banaszak, and N. P. Balsara, "50th anniversary perspective: Phase behavior of polymer solutions and blends," Macromolecules **50**, 3051–3065 (2017).
[49]S. Adhikari, M. A. Leaf, and M. Muthukumar, "Polyelectrolyte complex coacervation by electrostatic dipolar interactions," J. Chem. Phys. **149**(16), 163308 (2018).
[50]B. Hammouda, *Polymer Characteristics* (Springer, Berlin, Heidelberg, 1993), pp. 87–133.
[51]G. D. Wignall and Y. B. Melnichenko, "Recent applications of small-angle neutron scattering in strongly interacting soft condensed matter," Rep. Prog. Phys. **68**(8), 1761 (2005).
[52]K. J. Zhang, M. E. Briggs, R. W. Gammon, J. V. Sengers, and J. F. Douglas, "Thermal and mass diffusion in a semidilute good solvent-polymer solution," J. Chem. Phys. **111**(5), 2270–2282 (1999).